

Multi-band characterization of the hot Jupiters: WASP-5b, WASP-44b, and WASP-46b

M. Moyano^{1*}, L. A. Almeida^{2†}, C. von Essen³, F. Jablonski⁴, M. G. Pereira⁵

¹*Instituto de Astronomía, Universidad Católica del Norte, Av. Angamos 0610, Antofagasta, Chile.*

²*Instituto de Astronomia, Geofísica e Ciências Atmosféricas, Universidade de São Paulo,*

Rua do Matão 1226, Cidade Universitária São Paulo-SP, 05508-090, Brasil

³*Stellar Astrophysics Centre, Department of Physics and Astronomy, Aarhus University, Ny Munkegade 120, 8000, Aarhus C, Denmark*

⁴*Instituto Nacional de Pesquisas Espaciais/MCTI, Avenida dos Astronautas 1758, São José dos Campos, SP, 12227-010, Brasil*

⁵*Departamento de Física, Universidade Estadual de Feira de Santana, Av. Transnordestina, S/N, Feira de Santana, BA, 44036-900, Brasil*

Accepted XXXX. Received YYYYYY; in original form 2017 May

ABSTRACT

We have carried out a campaign to characterize the hot Jupiters WASP-5b, WASP-44b, and WASP-46b using multi-band photometry collected at the Observatório do Pico Dos Dias in Brazil. We have determined the planetary physical properties and new transit ephemerides for these systems. The new orbital parameters and physical properties of WASP-5b and WASP-44b are consistent with previous estimates. In the case of WASP-46b, there is some quota of disagreement between previous results. We provide a new determination of the radius of this planet and help clarify the previous differences. We also studied the transit time variations including our new measurements. No clear variation from a linear trend was found for the systems WASP-5b and WASP-44b. In the case of WASP-46b, we found evidence of deviations indicating the presence of a companion but statistical analysis of the existing times points to a signal due to the sampling rather than a new planet. Finally, we studied the fractional radius variation as a function of wavelength for these systems. The broadband spectrums of WASP-5b and WASP-44b are mostly flat. In the case of WASP-46b we found a trend, but further measurements are necessary to confirm this finding.

Key words: planetary systems - stars: fundamental parameters.

1 INTRODUCTION

Since the announcement of the discovery of the first exoplanets orbiting the pulsar PSR 1257+12 (Wolszczan & Frail 1992; Wolszczan 1994) and the subsequent discovery of an exoplanet around a main sequence star (Mayor & Queloz 1995), more than three thousand planets orbiting other stars have been detected (Schneider et al. 2011, see exoplanet.eu). An exoplanet’s orbit oriented along the line of sight provides unmatched access to a list of both planetary astrophysical properties and orbital elements. The favorable geometry of transiting extrasolar planets (TEPs) allows the measurement of the true planetary masses and radii provided some external constraints from stellar evolutionary theory or empirical stellar mass-radius relations (Southworth 2009). Moreover, if the stellar limb-darkening is assumed to be negligible, the density of the star can be measured directly from

the light curve alone (Seager & Mallén-Ornelas 2003). Additionally, some of the stellar light filters through the exoplanet atmosphere during transit, resulting in spectral footprints that may reveal characteristics of the exoplanetary atmosphere (e.g. Swain et al. 2010). TEPs allow for the first time to access an accurate ensemble of planetary properties, thus the accurate characterization of each system plays an important role for both the determination of fundamental parameters and recognition of astrophysically interesting targets for follow-up work such as Transit Timing Variation (Holman & Murray 2005; Holman et al. 2010, TTV) or atmospheric characterization (see e.g., Seager & Deming 2010).

Hot Jupiters (HJs) are a class of large and gaseous planets similar to Jupiter, but orbiting very close to their host stars. These characteristics make these objects easier to detect compared with low-mass planets at wider orbits. Despite the large number of HJs discovered fundamental questions about their formation and evolution are still under debate. The main scenarios proposed to explain their tight orbital

* E-mail: mmoyano@ucn.cl

† E-mail: leonardodealmeida.andrade@gmail.com

trajectories are the formation of orbits with a small inclination via disk migration, or very inclined orbits via high-eccentricity migration due to tidal dissipation caused by gravitational interactions with another companion (see e.g. Ford & Rasio 2008; Thies et al. 2011; Tutukov & Fedorova 2012; Valsecchi & Rasio 2014). Therefore, precise physical and geometrical parameters of HJs derived from optical and infrared photometry are essential to test the planetary formation and evolution theories as well as to distinguish different types of atmospheres (Sing et al. 2016).

In this paper we present precision relative photometry of three HJs: WASP-5b, WASP-44b and, WASP-46b (Anderson et al. 2008, 2012). WASP-5b is a Hot-Jupiter with a mass of $M_P = 1.64 M_J$ and a radius of $R_P = 1.17 R_J$ transiting a bright ($V = 12.3$ mag) G4V star on a 1.63 day orbit. WASP-44b has a mass of $M_P = 0.89 M_J$ and a radius of $R_P = 1.00 R_J$ orbiting a bright ($V = 12.9$ mag) G8V star with an orbital period of 2.42 day. WASP-46b is a massive ($M_P = 2.10 M_J$) hot Jupiter with a radius of $R_P = 1.31 R_J$ eclipsing a bright ($V = 12.9$ mag) G6V star on a 1.43 day orbit.

This paper is structured as follows: Section 2 describes the observations and the data reduction, Section 3 presents our results and analysis, and in Section 4 we discuss our results and state our conclusions.

2 OBSERVATIONS AND DATA REDUCTION

The observations were carried out using the facilities of the Observatório do Pico dos Dias (OPD/LNA), in Brazil¹. Transits of the planets WASP-5b, WASP-44b, and WASP-46b were observed on 2011 August, 2012 August, 2013 July, and 2013 August using the Andor iKon-L CCD cameras mounted on the 1.6-m and 0.6-m telescopes. These cameras provide plate scales of 0.18 and 0.34 arcsec/pixel, respectively. A summary of the collected data is reported in Table 1. In this table, N is the number of individual images obtained with integration time t_{exp} .

The basic data reduction was done using IRAF² tasks. We created a master median bias of typically ~ 100 bias frames for each observing night. A normalized master flat-field frame was obtained by combining and then normalizing ~ 30 dome flat-field images. We process the images by subtracting the master bias and then dividing by the normalized master flat frame.

The target fields are not crowded, thus we performed standard differential aperture photometry. The telescope tracking and pointing were not stable during the observations, thus we carefully placed the apertures in each image for both the target and the reference non-variable stars. The fluxes were extracted using an implementation of DAOPHOT (Stetson 1987). We experimented with different apertures and sky rings and kept those which resulted in the lowest standard deviation after subtracting the fitted transit model (see next section). This was an efficient way of both measuring the fit quality, due to the reduced number of out-of-transit observations, and discarding outliers. We iteratively

removed the outliers discarding measurements $3 \times \sigma$ away from the resulting model light curve (see next section). We repeated this process up to 3 times for each band which resulted in a maximum of removal of 1.5% of the data points and an average reduction of 10% in the residuals standard deviation. The final aperture values used to extract our light curves are listed in Table 1³.

3 ANALYSIS AND RESULTS

3.1 Light curve Analysis

To fit the light curves we used EXOFAST (Eastman, Gaudi, & Agol 2013). This software implements the Markov Chain Monte Carlo (MCMC) method to estimate and characterize the parameters' uncertainty distributions (Ford 2005, 2006) and the light curve models of Mandel & Agol (2002). To evolve the MCMC chains it uses the Differential Evolution MCMC method (Ter Braak 2006). We included at each MCMC step the background value at the central pixel, airmass, and CCD positions, thus ensuring these systematics are considered at each MCMC jump. In fact, these systematics were critical to fit properly our light curves in the cases of changes of the positions of our targets and references (see discussion below about our systematics). To include these parameters in the MCMC chains we considered a linear combination of the (x,y) pixel positions of the target's star centroid, the airmass, and the background value which was computed averaging the pixel values within a ring around the star. For each light curve we ran MCMC chains of maximum 100,000 iterations, and discarded the first 25,000 chains which eliminated any bias due to the starting conditions ("burn-in" process, Tegmark et al. 2004). To check their convergency, we divided the final 75,000 values into three, and computed the mean and standard deviation (best fit value and error) of the posterior distributions. If the derived values were consistent within 1 sigma errors, we considered the chains to be convergent. Since we fitted only transit data, we complemented our fits with spectroscopic information taken from Anderson et al. (2008, 2012); Triaud et al. (2010). We fixed the eccentricities to zero, as the radial velocity data is consistent with circular orbits.

EXOFAST uses a quadratic law to take into account the limb-darkening. Southworth (2008) proved this law is sufficient to model high quality ground-based light curves. We fitted both coefficients for each light curve. Espinoza & Jordán (2015) proved that this approach introduces bias just up to $\sim 1\%$ in R_p/R_* . EXOFAST adds a penalty term at each MCMC jump based on the tables of Claret & Bloemen (2011), thus constraining the fitted limb-darkening coefficients and preventing their values to be unphysical.

We calculated the standard deviation of the measurements after subtracting the fitted model (scatter) to assess the quality of the fit. The final scatter values are displayed on Table 1.

Light curves of planetary transits have systematic effects,

¹ <http://www.lna.br/opd/opd.html>

² <http://www.iraf.noao.edu>

³ The original light curves can be downloaded at http://www.iaucln.cl/Users/Max/PUBLIC/PAPER_OPD/

Table 1. Summary of the photometric observations presented in this work.

Target	UT Date	N	t_{exp} (s)	Telescope	Filter	Aperture(pixel)	Scatter(%) ^a	Slope Spectrum ^b
WASP-5b	2012 Aug 10	992	10	1.6-m	V	16.0	0.23	$(1.73 \pm 2.3) \times 10^{-5}$
	2012 Aug 10	362	40	0.6-m	I _C	9.0	0.26	
WASP-44b	2012 Aug 11	296	60	1.6-m	V	11.0	0.14	$(-1.07 \pm 11.1) \times 10^{-6}$
	2012 Aug 11	346	40	0.6-m	R _C	8.0	0.38	
	2012 Aug 11	200	60	0.6-m	I _C	5.0	0.40	
	2012 Aug 16	230	60	1.6-m	B	11.0	0.19	
	2013 Aug 01	832	08	1.6-m	I _C	7.0	0.24	
WASP-46b	2011 Aug 14	300	30	1.6-m	V	13.0	0.19	$(-2.31 \pm 1.77) \times 10^{-5}$
	2013 Jul 30	601	10	1.6-m	I _C	10.0	0.23	
	2013 Aug 02	361	15	1.6-m	R _C	14.0	0.17	

^a Standard deviation of the residuals after subtracting the fitted model

^b See section 3.5

the so called correlated “red noise” (Pont, Zucker, & Queloz 2006). To quantify this noise we used the residual permutation method (Jenkins, Caldwell, & Borucki 2002, RPM) implemented in the transit analysis package JKTEBOP (Southworth 2008). In this method, the residuals around the best fit are shifted point by point along the observations and a new fit is performed (if a residual is shifted after the end it is moved to the beginning). This is done for all observational data points. From the resultant distribution the errors are calculated as in the MCMC case. These uncertainties are a way to quantify the systematics present in our data. We found that the uncertainties determined by the RPM are in most cases similar to the MCMC case for the data taken with the 1.6 $- m$ telescope (there just a couple of extreme cases where the RPM uncertainties are slightly larger). In the case of data taken with the 0.6 $- m$ telescope, the RPM uncertainties are up to three times the MCMC uncertainties, so the systematics are stronger in this case. This is in part explained because the pointing of the 0.6 $- m$ telescope changes more drastically (drift of 90 pixels for every 20 minutes of observing time), thus target and references are placed on different CCD positions, therefore increasing the systematics due to changes in quantum efficiency. Additionally, the 0.6 $- m$ has no guiding system. The 1.6 $- m$ telescope has a guiding system and therefore a better pointing. As pointed out before, these changes of position were taken into account at each MCMC iteration.

We also fitted the light curves with JKTEBOP using MCMC simulations (using an approach similar to that of EXOFAST). This served as a consistency check of our EXOFAST results. We found the results to be consistent with each other within one standard deviation. We preferred EXOFAST results because it implements at each MCMC jump a penalty term taking into account the decorrelation parameters. As stated before, taking into account the systematics present in our data is critical for improving the final results and to properly characterize the uncertainties. As a final consistency check, we also analyzed our light curves using the graphical transit analysis interface TAP (Gazak et al. 2012). We also found the results to be consis-

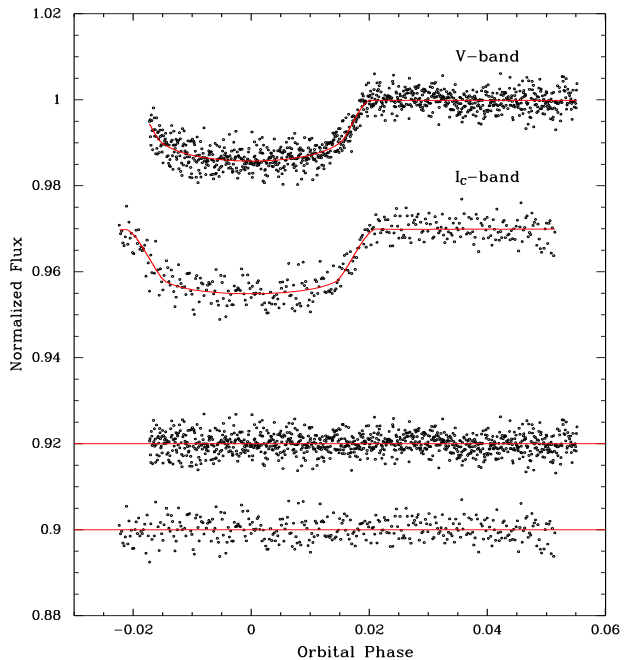


Figure 1. WASP-5b light curves. From top to bottom the V- and I_C-band light curves respectively. The red curves are the best fits superimposed. The residuals of the fitted model are displayed at the bottom. The displayed light curves are decorrelated using the parameters described in Section 3.1.

tent with EXOFAST within one standard deviation. This is expected, because TAP uses EXOFAST (Gazak et al. 2012), but iterates the MCMC chains using a wavelet-based likelihood (Carter & Winn 2009). All the results presented in this paper come from the EXOFAST results and the other tools were used just as an initial consistency check. Figures 1, 2 and 3 show the resultant light curves of WASP-5b, WASP-44b, and WASP-46b, respectively. In all cases, the scatter of the residuals was better than 0.4%.

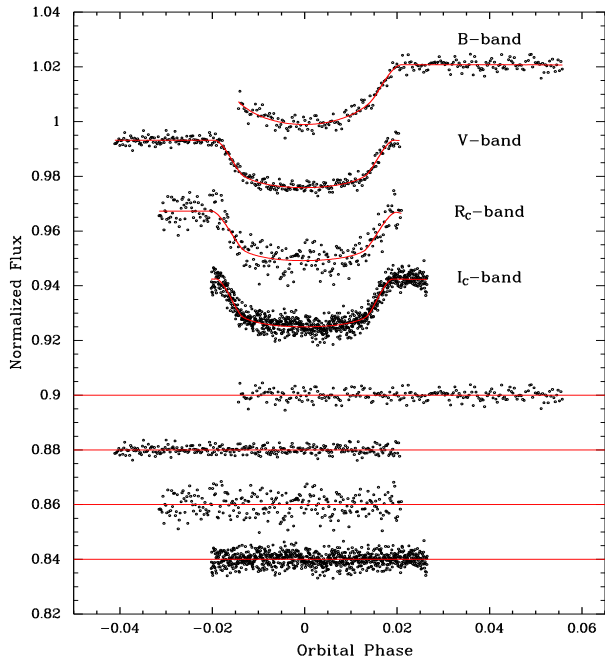


Figure 2. WASP-44b light curves. From top to bottom the B-, V-, R_C -, and I_C -band light curves respectively. The red curves are the best fits superimposed. The residuals of the fitted model are displayed at the bottom. The displayed light curves are decorrelated using the parameters described in Section 3.1.

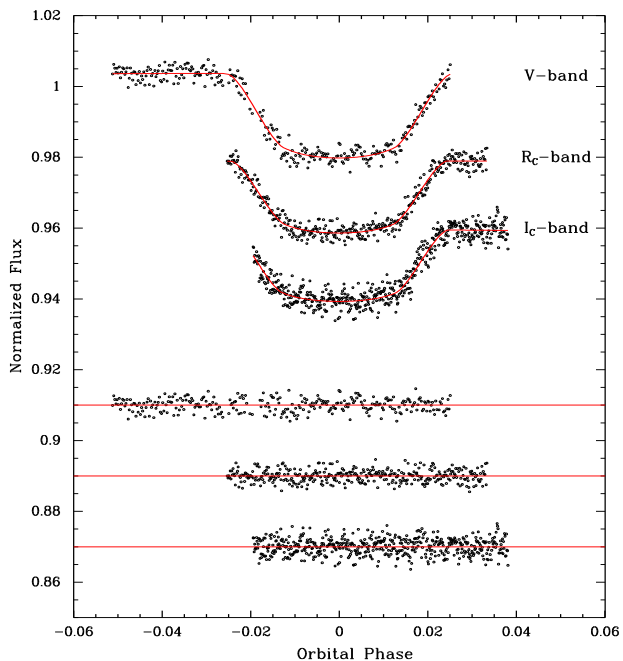


Figure 3. WASP-46b light curves. From top to bottom the V-, R_C -, and I_C -band light curves respectively. The red curves are the best fits superimposed. The residuals of the fitted model are displayed at the bottom. The displayed light curves are decorrelated using the parameters described in Section 3.1.

3.2 System Parameters

Tables 2, 3, and 4 show the determined parameters in all bands for the planets WASP-5b, WASP-44b, and WASP-46b, respectively. As mentioned before, the quality of the light curves taken with the 1.6-m telescope is better, so we preferred those for I_C -band results of WASP-44b. Thus, all the results presented in this paper refer to the I_C -band taken with the 1.6-m telescope for the WASP-44b system. The inclination of the system and the orbital semi-major axis are independent of wavelength, thus a unique value can be determined. We calculated a final value using as weight the inverse square of the individual uncertainties. Table 5 shows the results and previous estimates for the planets WASP-5b, WASP-44b, and WASP-46b, respectively. Our values are consistent with previous results for these planets. We have improved the value of the inclination for WASP-5b and the normalized semi-major axis a/R_* for WASP-46b.

3.3 Transit ephemerides

We determined the transit ephemerides of WASP-5b, WASP-44b, and WASP-46b assuming linear ephemerides. We combined our mid-transit times with all measurements published in the literature including the times available on TRESCA⁴. We selected all the entries on TRESCA with a data quality index better than 3 and we inspected each light curve for possible systematics. We converted all measurements to barycentric dynamical time BJD(TDB) using the time routines from Eastman, Siverd, & Gaudi (2010). For the TRESCA transit times we convert their JD(UTC) to BJD(TDB) which is more precise than converting directly their HJD(TT) to BJD(TDB). To fit the mid-transit times we used the expression $T_{\min} = T_0 + E \times P_b$, where T_{\min} are the predicted mid-transit times, T_0 is a fiducial epoch, E is the cycle count from T_0 , and P_b is the planetary orbital period. We use a simple linear regression to fit the linear ephemerides equation to the mid-transit times. The best solutions obtained were:

$$T_{\min} = 2454375.6251(2) + E \times 1.6284305(2), \quad (1)$$

$$T_{\min} = 2455434.3774(7) + E \times 2.423807(3), \quad (2)$$

$$T_{\min} = 2455392.3139(9) + E \times 1.430375(2), \quad (3)$$

for WASP-5b, WASP-44b, and WASP-46b, respectively.

3.4 Transit timing variations

The mid-transit times and the residuals from the fit are shown in Figure 5 and listed in Tables 6, 7, and 8. In the absence of transit timing variations (Holman & Murray 2005; Holman et al. 2010) we would expect no statistically significant deviations of the derived [O (*observed*) - C (*calculated*)] values from zero. To test the truthfulness of this we computed χ_{red}^2 for the three systems and found $\chi_{\text{red,WASP-5b}}^2 = 2.1$, $\chi_{\text{red,WASP-44b}}^2 = 3.2$ and

⁴ The TRansiting ExoplanetS and CAndidates (TRESCA) website can be found at <http://var2.astro.cz/EN/tresca/index.php>

Table 2. Planetary parameters of WASP-5b.

Symbol	Parameter	V	I _C
$a \dots$	Semi-major axis (AU).....	$0.02789^{+0.00059}_{-0.00058}$	$0.02793^{+0.00056}_{-0.00055}$
$R_P \dots$	Radius (R_J).....	$1.126^{+0.100}_{-0.082}$	$1.240^{+0.085}_{-0.081}$
R_P/R_\star	Planet/star radius ratio.....	$0.1114^{+0.0015}_{-0.0015}$	$0.1158^{+0.0018}_{-0.0017}$
$T_{eq} \dots$	Equilibrium Temperature (K).....	1753^{+70}_{-62}	1765^{+64}_{-62}
$\langle F \rangle \dots$	Incident flux ($10^9 \text{ erg s}^{-1} \text{ cm}^{-2}$).....	$2.14^{+0.37}_{-0.29}$	$2.21^{+0.34}_{-0.29}$
$T_C \dots$	Time of mid-transit(BJD _{TDB} -2450000)	$6150.61479^{+0.00050}_{-0.00056}$	$6150.61396^{+0.00054}_{-0.00057}$
$u_1 \dots$	linear limb-darkening coeff.....	0.484 ± 0.049	$0.285^{+0.048}_{-0.050}$
$u_2 \dots$	quadratic limb-darkening coeff.....	0.283 ± 0.052	$0.290^{+0.048}_{-0.049}$
$i \dots$	Inclination (degrees).....	$86.1^{+1.8}_{-1.4}$	$84.54^{+0.74}_{-0.66}$
$\delta \dots$	Transit depth.....	$0.01155^{+0.00056}_{-0.00051}$	$0.01373^{+0.00053}_{-0.00052}$
$T_{14} \dots$	Total duration (days).....	$0.0978^{+0.0018}_{-0.0016}$	$0.0935^{+0.0025}_{-0.0023}$

Table 3. Planetary parameters of WASP-44b.

Symbol	Parameter	V	B	R _C	I _C
$a \dots$	Semi-major axis (AU).....	0.0352 ± 0.0014	$0.0328^{+0.0016}_{-0.0015}$	0.0354 ± 0.0016	$0.0349^{+0.0015}_{-0.0016}$
$R_P \dots$	Radius (R_J).....	$1.12^{+0.10}_{-0.11}$	$1.08^{+0.15}_{-0.13}$	1.18 ± 0.13	$1.121^{+0.080}_{-0.081}$
R_P/R_\star	Planet/star radius ratio.....	$0.1224^{+0.0013}_{-0.0013}$	$0.1346^{+0.0031}_{-0.0031}$	$0.1256^{+0.0033}_{-0.0032}$	$0.1246^{+0.0025}_{-0.0025}$
$T_{eq} \dots$	Equilibrium Temperature (K).....	1390 ± 120	1200^{+120}_{-130}	1410^{+140}_{-130}	1360 ± 120
$\langle F \rangle \dots$	Incident flux ($10^9 \text{ erg s}^{-1} \text{ cm}^{-2}$).....	$0.85^{+0.33}_{-0.25}$	$0.46^{+0.23}_{-0.14}$	$0.89^{+0.40}_{-0.29}$	$0.78^{+0.31}_{-0.23}$
$T_C \dots$	Time of mid-transit(BJD _{TDB} -2450000)	$6151.82559^{+0.00046}_{-0.00045}$	$6156.6694^{+0.0014}_{-0.0019}$	$6151.82415^{+0.0010}_{-0.00095}$	6505.70010 ± 0.00025
$u_1 \dots$	linear limb-darkening coeff.....	$0.493^{+0.094}_{-0.084}$	$0.932^{+0.089}_{-0.12}$	$0.378^{+0.10}_{-0.089}$	$0.331^{+0.071}_{-0.070}$
$u_2 \dots$	quadratic limb-darkening coeff.....	$0.222^{+0.076}_{-0.088}$	$-0.044^{+0.12}_{-0.095}$	$0.252^{+0.066}_{-0.074}$	$0.252^{+0.061}_{-0.063}$
$i \dots$	Inclination (degrees).....	$86.13^{+0.81}_{-0.58}$	$86.89^{+1.2}_{-0.85}$	$85.85^{+1.2}_{-0.60}$	$86.23^{+0.56}_{-0.48}$
$\delta \dots$	Transit depth.....	$0.01501^{+0.00065}_{-0.00079}$	$0.0171^{+0.0015}_{-0.0014}$	0.0163 ± 0.0012	$0.01542^{+0.00071}_{-0.00070}$
$T_{14} \dots$	Total duration (days).....	0.0942 ± 0.0016	$0.0963^{+0.0042}_{-0.0038}$	$0.0937^{+0.0032}_{-0.0030}$	$0.09516^{+0.00099}_{-0.00095}$

$\chi^2_{\text{red, WASP-46b}} = 61.8$. Although the three values are sufficiently large to suspect the presence of TTVs, values around $\chi^2_{\text{red}} \sim 3$ have created already some disagreement between authors (see e.g., von Essen et al. 2013 but then Mislis et al. 2015). Nonetheless, WASP-46b's χ^2_{red} value is large enough to suspect TTVs. To further investigate this we applied a Lomb-Scargle periodogram (Lomb 1976; Scargle 1982; Zechmeister & Kürster 2009) to the (O-C) values. The derived false alarm probabilities (FAP) are $\text{FAP}_{\text{WASP-5b}} = 0.64$, $\text{FAP}_{\text{WASP-44b}} = 0.17$ and $\text{FAP}_{\text{WASP-46b}} = 0.0002$, placing again WASP-46b as a good candidate for TTVs. The power spectrum of WASP-46b's periodogram has a peak at $0.0034 \pm 0.0004 \text{ c/d}$ (cycles per day), which corresponds to ~ 295 days. The frequency and error were computed fitting a Gaussian profile to the maximum peak of the periodogram. As a measurement of the amplitude of WASP-46's (O-C) diagram we used its standard deviation, with a value of 250.7 seconds. We finally re-determined the FAP of the TTV signal but using a bootstrap resampling method. For this, we randomly permuted the mid-transit values along with their errors 5×10^5 times, but leaving the epochs fixed. At each iteration we calculated a Lomb-Scargle periodogram from the permuted (O-C) diagram. We estimated the FAP as the frequency with which the highest power in the scrambled periodogram exceeds the maximum power in the original periodogram. Using this more reliable technique, the re-estimated FAP for WASP-46b is 0.04, inconsistent with the one computed in the usual

way but still low. Finally, to characterize WASP-46b's TTVs we computed the spectral window of its (O-C) diagram. If the signal is associated with the sampling rather than to the true TTV signal, then the spectral window power spectrum should have a similar peak around 0.0034 c/d . This was the case. We found one single and isolated peak at $0.0026 \pm 0.0004 \text{ c/d}$, just consistent with the previously computed TTV signal at the $1\text{-}\sigma$ level (see Figure 4). Although the TTV amplitude is significantly large, we notice that the more distant an (O-C) data point is from zero, the larger its error bar is. We therefore advise caution to readers who may want to interpret these TTVs.

3.5 Broadband spectrum

Multi-band transit observations allow to study the fractional radii variation as a function of the wavelength. The planetary radius R_p derived from transit observations may vary with the wavelength, as it can appear slightly larger when observed at wavelengths where the atmosphere contains strong opacity sources (Burrows et al. 2000; Seager & Sasselov 2000). These changes are at first approximation the broad-band transmission spectrum (e.g. Nikolov et al. 2013). We fitted our light curves again, but now we introduced as priors the calculated common parameters shown in Table 5 and the orbital periods. This improves the quality of the fractional radius determination. The improved results for this parameter are shown in Ta-

Table 4. Planetary parameters of WASP-46b.

Symbol	Parameter	V	R _C	I _C
a ...	Semi-major axis (AU)	0.02421 ± 0.00052	$0.02414^{+0.00055}_{-0.00054}$	0.02407 ± 0.00055
R_P .	Radius (R_J).....	$1.338^{+0.064}_{-0.062}$	$1.230^{+0.052}_{-0.051}$	$1.209^{+0.074}_{-0.072}$
R_P/R_*	Planet/star radius ratio.....	$0.1507^{+0.0017}_{-0.0017}$	$0.14109^{+0.00099}_{-0.00099}$	$0.1403^{+0.0021}_{-0.0022}$
T_{eq} .	Equilibrium Temperature (K).....	1678^{+51}_{-53}	1657^{+53}_{-52}	1641 ± 58
$\langle F \rangle$.	Incident flux ($10^9 \text{ erg s}^{-1} \text{ cm}^{-2}$)	$1.80^{+0.23}_{-0.22}$	$1.71^{+0.23}_{-0.20}$	$1.65^{+0.25}_{-0.22}$
T_C ..	Time of mid-transit (BJD _{TDB} -2450000)	$5788.52807^{+0.00032}_{-0.00030}$	$6506.57629^{+0.00023}_{-0.00025}$	6503.71529 ± 0.00034
u_1 ..	linear limb-darkening coeff.....	$0.384^{+0.055}_{-0.053}$	$0.345^{+0.055}_{-0.054}$	$0.307^{+0.054}_{-0.053}$
u_2 ..	quadratic limb-darkening coeff.....	$0.241^{+0.053}_{-0.054}$	0.275 ± 0.051	$0.287^{+0.049}_{-0.052}$
i	Inclination (degrees)	$82.87^{+0.34}_{-0.32}$	$82.73^{+0.33}_{-0.32}$	$82.92^{+0.46}_{-0.41}$
δ	Transit depth.....	$0.02293^{+0.00082}_{-0.00076}$	$0.01976^{+0.00045}_{-0.00043}$	$0.01943^{+0.0010}_{-0.00095}$
T_{14} .	Total duration (days).....	$0.0727^{+0.0014}_{-0.0013}$	$0.06994^{+0.0010}_{-0.00094}$	0.0703 ± 0.0017

Table 5. Weighted mean of common parameters for WASP-5b, WASP-44b, and WASP-46b

WASP-5b				
Parameter	This work	Southworth (2009)	Triaud et al. (2010)	Fukui et al. (2011)
i[degrees]	84.77 ± 0.68	85.8 ± 1.1	$86.2^{+0.8}_{-1.7}$	$85.58^{+0.81}_{-0.76}$
a/R_*	5.54 ± 0.19	$5.41^{+0.17}_{-0.18}$	$5.49^{+0.37}_{-0.12}$	5.37 ± 0.15
WASP-44b				
Parameter	This work	Anderson et al. (2012)	Mancini et al. (2013)	Turner et al. (2016)
i[degrees]	86.18 ± 0.37	$86.02^{+1.11}_{-0.86}$	86.59 ± 0.18	
a/R_*	8.10 ± 0.20	$8.05^{+0.66}_{-0.52}$	8.58 ± 0.3	$8.33^{+0.09}_{-0.14}$
WASP-46b				
Parameter	This work	Anderson et al. (2012)	Ciceri et al. (2016)	
i[degrees]	82.82 ± 0.21	82.63 ± 0.38	82.80 ± 0.17	
a/R_*	5.76 ± 0.09	5.74 ± 0.15	5.85 ± 0.12^a	

^a Value calculated using the reported values of Ciceri et al. (2016) (propagating the lowest reported uncertainties for a and R_*)

bles 2, 3, and 4 for WASP-5b, WASP-44b, and WASP-46b, respectively. Figures 6, 7, and 8 show the resulting fractional radii variation as a function of wavelength using our measurements (red squares) and the ones available in the literature (pink squares) for the planets WASP-5b, WASP-44b, and WASP-46b, respectively. The horizontal error bars represent the FWHM of the used filters. The superimposed dotted green line in these figures is the linear fit using only our measurements constraining the fit to cross our measurement with the longest wavelength. We calculated the slopes of these lines to investigate some trends in our measurements. The values of the slopes are listed in Table 1.

In the case of WASP-5b, there are not enough measurements to have an unambiguous view to describe a conclusive scenario for any correlation between the planetary radius and wavelength (e.g. Jha et al. 2000). In the case of WASP-44b, our values are consistent with a flat spectrum similar to that of Turner et al. (2016) (see their figure 9). Our calculated slope (see Table 1) is consistent with zero. A flat spectrum is indicative of the presence of clouds in the upper atmosphere which prevent observation of any

spectral features (Turner et al. 2016; Seager & Sasselov 2000). In the case of WASP-46b, we see indications of an increase of radius (4σ) at the shortest wavelengths, a hint of possible Rayleigh scattering in the atmosphere of this planet (Lecavelier Des Etangs et al. 2008). We notice that Ciceri et al. (2016) found no strong evidence of Rayleigh scattering in the atmosphere of WASP-46b (see their figure 8). They found a slope with maximum inclination of $m = -1.17 \times 10^{-5}$ for WASP-46b (1/2 of our slope, see Table 1). Although there is rotational modulation on this system (Anderson et al. 2012), the stellar activity is not sufficient to explain this difference, so further measurements are necessary confirm or rule out this scenario. We also notice that the V-band light curve of WASP-46b is missing the flat part after egress (see Figure 3), thus preventing from strongly constraining the baseline value, although our measurement is consistent within 2σ with that of Anderson et al. (2012). As pointed out by Gibson (2014), choosing an incorrect noise model might artificially lower the uncertainties which is equivalent to getting the normalization of the light curve wrong, thus such high slope

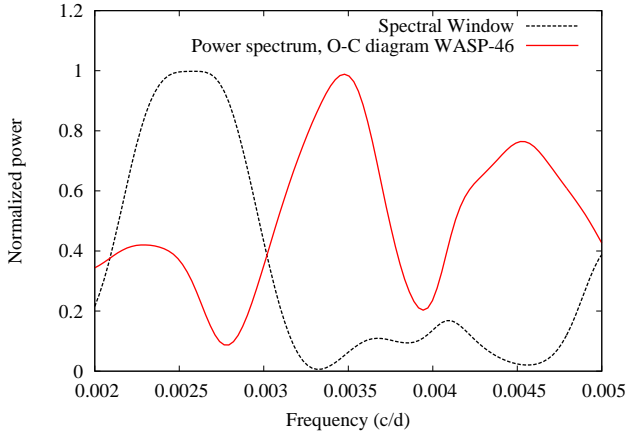


Figure 4. The figure shows, in a red continuous line, the periodogram of WASP-46 TTVs zoomed-in around the maximum power. On top of this, the spectral window (i.e., the periodicity induced by the sampling of the data) is plotted in black dashed lines. For a better comparison, both periodograms have been normalized to their respective maximum values.

Table 6. Mid-transit times for WASP-5b

Cycle	T(BJD _{TDB}) 2450000 +	(O-C) s	Reference
-264	3945.71962±0.00093	15	Gillon et al. 2008
-7	4364.2283±0.0013	191	Gillon et al. 2008
0	4375.62535±0.00026	22	Gillon et al. 2008
5	4383.7675±0.0004	-36	Anderson et al. (2008)
7	4387.02275±0.0010	-164	Anderson et al. (2008)
160	4636.17459±0.00079	53	Fukui et al. (2011)
199	4699.68303±0.00040	22	¹
204	4707.82523±0.00023	26	Southworth et al. (2009)
204	4707.82465±0.00052	-23	¹
218	4730.62243±0.00031	-45	Southworth et al. (2009)
218	4730.62301±0.00075	5	¹
237	4761.56356±0.00047	37	¹
244	4772.96212±0.00074	-2	Fukui et al. (2011)
245	4774.59093±0.00030	31	¹
253	4787.61792±0.00069	-9	¹
387	5005.82714±0.00036	-49	¹
414	5049.79540±0.00080	6	¹
430	5075.84947±0.00056	-64	Dragomir et al. (2011)
432	5079.10830±0.00075	105	Fukui et al. (2011)
451	5110.04607±0.00087	-102	Fukui et al. (2011)
459	5123.07611±0.00079	121	Fukui et al. (2011)
463	5129.58759±0.00042	-72	¹
607	5364.0815±0.0011	-79	Fukui et al. (2011)
615	5377.10955±0.00091	-27	Fukui et al. (2011)
659	5448.75927±0.0010	-133	Dragomir et al. (2011)
934	5896.58124±0.00046	177	TRESCA
1074	6124.55945±0.00042	-2	TRESCA
1082	6137.58653±0.00037	-33	TRESCA
1090	6150.61396±0.00057	-34	This study
1090	6150.61479±0.00056	37	This study
1536	6876.89438±0.00027	1	TRESCA
1547	6894.80707±0.0003415	-3	TRESCA
1547	6894.80726±0.00042	14	TRESCA
1593	6969.71467±0.00024	-20	TRESCA

¹ Hoyer, Rojo, & López-Morales (2012);

could be in part explained by the lack of observations after egress. We therefore advise caution to readers who may want to interpret this significant variation of the broadband spectrum of WASP-46b. Although we recognize the V-band planetary to star radii ratio of WASP-46b is significantly larger than in the other bands, additional measurements

Table 7. Mid-transit times for WASP-44b

Cycle	T(BJD _{TDB}) 2450000 +	(O-C) s	Reference
0	5434.37637 ± 0.00040	-89	Anderson et al. (2012)
8	5453.76639 ± 0.00042	-127	Anderson et al. (2012)
154	5807.64374 ± 0.00013	1	Mancini et al. (2013)
157	5814.91731 ± 0.00150	187	Evans P.(TRESCA)
163	5829.45485 ± 0.00245	-271	Lomoz F.(TRESCA)
163	5829.46110 ± 0.00163	268	Lomoz F.(TRESCA)
166	5836.72905 ± 0.00020	-31	Mancini et al. (2013)
166	5836.72979 ± 0.00030	33	Mancini et al. (2013)
166	5836.72900 ± 0.00020	-35	Mancini et al. (2013)
166	5836.72928 ± 0.00015	-11	Mancini et al. (2013)
168	5841.57719 ± 0.00035	14	Mancini et al. (2013)
168	5841.57757 ± 0.00046	47	Mancini et al. (2013)
168	5841.57684 ± 0.00028	-16	Mancini et al. (2013)
168	5841.57769 ± 0.00031	57	Mancini et al. (2013)
286	6127.58626 ± 0.00048	-2	Sauer T.(TRESCA)
296	6151.82555 ± 0.00060	103	This study
296	6151.8242 ± 0.0010	-18	This study
296	6151.82559 ± 0.00045	106	This study
298	6156.6694 ± 0.0017	-222	This study
442	6505.7001 ± 0.0002	-11	This study
466	6563.87407 ± 0.00102	213	Evans P.(TRESCA)
493	6629.31154 ± 0.00127	-247	Ren R.(TRESCA)

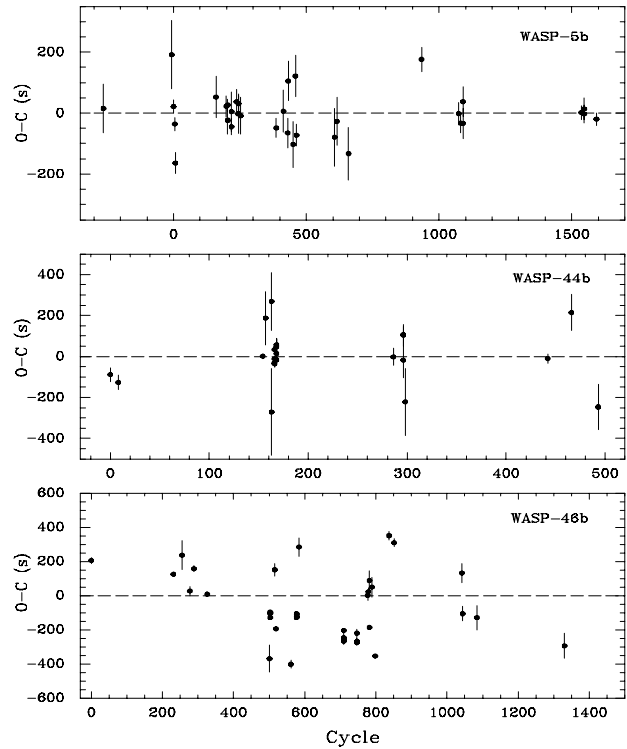


Figure 5. The panels from the top to bottom show the (O-C) diagrams for WASP-5b, WASP-44b, and WASP-46b, respectively.

will be needed to confirm this finding due to our lack of observations after egress.

As an alternative way of quantifying how much do the planetary to star radii ratio and wavelength correlate to each other, we made use of the Pearson's correlation coefficient, r . The derived values are as follows: $r_{WASP-44b} = -0.61$, $r_{WASP-46b} = 0.11$, and $r_{WASP-5b} = 0.05$. These coefficients indicate that there is no correlation between the

Table 8. Mid-transit times for WASP-46b.

Cycle	T(BJD _{TDB}) 2450000 +	(O-C) s	Reference
0	5392.31628 ± 0.00020	206	Anderson et al. (2012)
231	5722.73197 ± 0.00013	125	Ciceri et al. (2016)
255	5757.06225 ± 0.00098	235	TRESCA
277	5788.52807 ± 0.00030	25	This work
289	5805.69409 ± 0.00020	157	Ciceri et al. (2016)
326	5858.61624 ± 0.00011	8	Ciceri et al. (2016)
501	6108.92750 ± 0.00091	-370	TRESCA
503	6111.79133 ± 0.00011	-103	Ciceri et al. (2016)
503	6111.79141 ± 0.00013	-97	Ciceri et al. (2016)
503	6111.79132 ± 0.00013	-104	Ciceri et al. (2016)
503	6111.79102 ± 0.00013	-130	Ciceri et al. (2016)
516	6130.38914 ± 0.00042	150	TRESCA
519	6134.67627 ± 0.00016	-195	TRESCA
561	6194.74962 ± 0.00027	-402	Ciceri et al. (2016)
577	6217.63904 ± 0.00013	-107	Ciceri et al. (2016)
577	6217.63892 ± 0.00011	-117	Ciceri et al. (2016)
577	6217.63883 ± 0.00010	-125	Ciceri et al. (2016)
577	6217.63877 ± 0.00012	-130	Ciceri et al. (2016)
584	6227.65619 ± 0.00062	284	TRESCA
710	6407.87778 ± 0.00014	-205	Ciceri et al. (2016)
710	6407.87730 ± 0.00033	-246	Ciceri et al. (2016)
710	6407.87711 ± 0.00017	-262	Ciceri et al. (2016)
710	6407.87705 ± 0.00021	-268	Ciceri et al. (2016)
747	6460.80084 ± 0.00016	-275	Ciceri et al. (2016)
747	6460.80090 ± 0.00020	-270	Ciceri et al. (2016)
747	6460.80147 ± 0.00028	-221	Ciceri et al. (2016)
747	6460.80092 ± 0.00025	-269	Ciceri et al. (2016)
777	6503.71529 ± 0.00034	1	This work
779	6506.57629 ± 0.00025	23	This work
782	6510.86498 ± 0.00013	-187	Ciceri et al. (2016)
782	6510.86816 ± 0.00067	87	TRESCA
789	6520.88034 ± 0.00067	49	TRESCA
798	6533.74905 ± 0.00013	-354	Ciceri et al. (2016)
837	6589.54183 ± 0.00031	350	TRESCA
851	6609.56661 ± 0.00027	309	TRESCA
1042	6882.76617 ± 0.00065	131	TRESCA
1044	6885.62416 ± 0.00049	-107	TRESCA
1084	6942.83890 ± 0.00083	-130	TRESCA
1330	7294.70924 ± 0.00085	-295	TRESCA

wavelength and planetary to star radii ratio for the systems WASP-5b and WASP-46b (values are close to zero). The coefficient $r_{WASP-44b}$ indicates that there is a significant anti-correlation for WASP-44b. In any case, we consider it unlikely that the amplitude of the variability in WASP-44b could vary with wavelength by more than 10 scale heights, a sensible limit for expected variability when Rayleigh scattering is being investigated (Sing et al. 2016).

4 SUMMARY

In this paper we have presented multi-band photometry of three hot Jupiters: WASP-5b, WASP-44b, and WASP-46b. The data were collected as part of an observational program to characterize hot Jupiters which has been carried out with the facilities of the Pico dos Dias Observatory in Brazil. We performed a detailed analysis of the planetary transits using the following programs: EXOFAST (Eastman, Gaudi, & Agol 2013), TAP (Gazak et al. 2012), and, JKTEBOP (Southworth 2008). Using observations in the V -, B -, R_C -, and I_C -bands we were able to improve the geometrical and physical parameters of WASP-5b and WASP-46b (see Tables 2 and 4), in particular the ratio between the semi-major axis and the stellar radius for WASP-46b $a/R_* = 5.76 \pm 0.09$. The parameters we derived are consistent with previous studies (see Table 5)

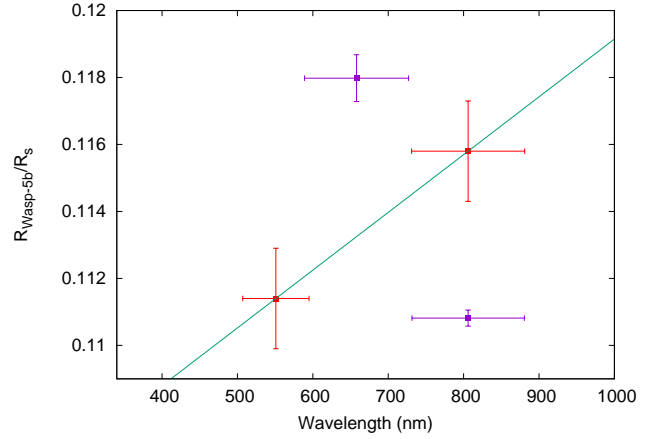


Figure 6. Planet to star radius of WASP-5b as a function of the observed band. The red squares are our measurements and the purple squares are the ones available in the literature. The green line is a linear fit to our measurements (see text).

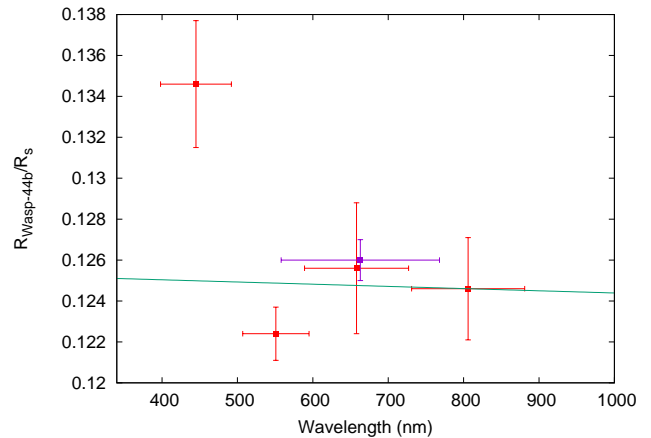


Figure 7. Planet to star radius of WASP-44b as a function of the observed band. Plotted as per the description for Figure 6.

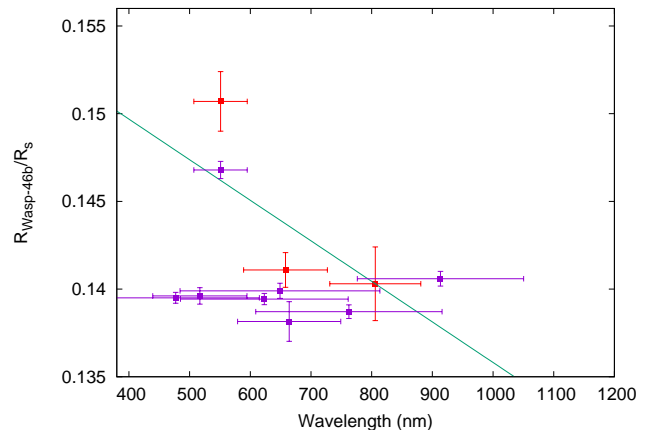


Figure 8. Planet to star radius of WASP-46b as a function of the observed band. Plotted as per the description for Figure 6.

We obtained improved linear ephemerides for WASP-5b, WASP-44b, and WASP-46b using our mid-transit times measurements together with all the other measurements available in the literature (see Section 3.3). The analysis of the residuals from the linear fit, the (O-C) diagram, doesn't show a clear indication of transit timing variation for WASP-5b and WASP-44b (see Figure 5). The (O-C) diagram of WASP-46b shows variation with a semi-amplitude of ~ 10 min. We proved this variation is most likely due to the sampling of the observations, but further additional transit time measurements of this system are necessary to secure this finding.

Finally, we studied the variation with wavelength of the planet to star radius for WASP-5b, WASP-44b, and WASP-46b. We don't have enough measurements to describe the broad-band spectrum of WASP-5b. In the case of WASP-44b, our values are consistent with a flat spectrum similar to that of previous studies. In the case of WASP-46b, we found marginal evidence of Rayleigh scattering which is not in agreement with a previous study. Further measurements are necessary to confirm or rule out this finding.

ACKNOWLEDGEMENTS

M. Moyano thanks Joseph Carson and an anonymous referee for some helpful suggestions and for a critical reading of the original version of the paper. L. A. Almeida acknowledges support from CAPES and Fundação de Amparo à Pesquisa do Estado de São Paulo - FAPESP (2013/18245-0 and 2012/09716-6). C. von Essen acknowledges funding for the Stellar Astrophysics Centre, provided by The Danish National Research Foundation (Grant DNR106).

REFERENCES

Anderson D. R., et al., 2008, MNRAS, 387, L4
 Anderson D. R., et al., 2012, MNRAS, 422, 1988
 Burrows A. et al., 2000, ApJ, 534, L97
 Carter J. A., Winn J. N., 2009, ApJ, 704, 51
 Charbonneau D., Brown T. M., Latham D. W., Mayor M., 2000, ApJ, 529, L45
 Ciceri S., et al., 2016, MNRAS, 456, 990
 Claret A., Bloemen S., 2011, A&A, 529, A75
 Dragomir D., et al., 2011, AJ, 142, 115
 Eastman J., Siverd R., Gaudi B. S., 2010, PASP, 122, 935
 Eastman J., Gaudi B. S., Agol E., 2013, PASP, 125, 83
 Espinoza N., Jordán A., 2015, MNRAS, 450, 1879
 Ford E. B., 2005, AJ, 129, 1706
 Ford E. B., 2006, ApJ, 642, 505
 Ford, E. B., Rasio, F. A., 2008, ApJ, 686, 621
 Fukui A., et al., 2011, PASJ, 63, 287
 Gazak J. Z., Johnson J. A., Tonry J., Dragomir D., Eastman J., Mann A. W., Agol E., 2012, AdAst, 2012,
 Gibson N. P., 2014, MNRAS, 445, 3401
 Holman M. J., Murray N. W., 2005, Sci, 307, 1288
 Holman M. J., et al., 2010, Sci, 330, 51
 Hoyer S., Rojo P., López-Morales M., 2012, ApJ, 748, 22
 Jha S. et al., 2000, ApJ, 540, L45
 Jenkins J. M., Caldwell D. A., Borucki W. J., 2002, ApJ, 564, 495

Lecavelier Des Etangs A., Vidal-Madjar A., Désert J.-M., Sing D., 2008, A&A, 485, 865
 Lomb N. R., 1976, Ap&SS, 39, 447
 Mancini L., et al., 2013, MNRAS, 430, 2932
 Mandel K., Agol E., 2002, ApJ, 580, L171
 Mayor M., Queloz D., 1995, Nature, 378, 355
 Mislis D., et al., 2015, MNRAS, 448, 2617
 Nikolov N., Chen G., Fortney J. J., Mancini L., Southworth J., van Boekel R., Henning T., 2013, A&A, 553, A26
 Pont F., Zucker S., Queloz D., 2006, MNRAS, 373, 231
 Scargle J. D., 1982, ApJ, 263, 835
 Schneider J., Dedieu C., Le Sidaner P., Savalle R., Zolotukhin I., 2011, A&A, 532, A79
 Seager S., Sasselov D. D., 2000, ApJ, 537, 916
 Seager S., Mallén-Ornelas G., 2003, ApJ, 585, 1038
 Seager S., Deming D., 2010, ARA&A, 48, 631
 Sing, D. K., Fortney, J. J., Nikolov, N., et al. 2016, Nature, 529, 59
 Southworth J., 2008, MNRAS, 386, 1644
 Southworth J., 2009, MNRAS, 394, 272
 Southworth J., et al., 2009, MNRAS, 396, 1023
 Stetson P. B., 1987, PASP, 99, 191
 Swain M. R., et al., 2010, Natur, 463, 637
 Tegmark M., et al., 2004, PhRvD, 69, 103501
 ter Braak, C. J. F. 2006, Statistics and Computing, 16, 239
 Thies, I., et al., 2011, MNRAS, 417(3), 1817
 TriAUD A. H. M. J., et al., 2010, A&A, 524, A25
 Turner J. D., et al., 2016, MNRAS, 459, 789
 Tutukov, A. V., Fedorova, A. V., 2012, Astronomy Reports, 56, 305
 Valsecchi, F., Rasio, F. A., 2014, ApJ 786, 102
 von Essen C., Schröter S., Agol E., Schmitt J. H. M. M., 2013, A&A, 555, A92
 Wolszczan, A., Frail D. A., 1992, Nature, 355, 145
 Wolszczan, A., 1994, Science, 264, 538
 Zechmeister M., Kürster M., 2009, A&A, 496, 577